ACS Sustainable Chemistry & Engineering

Research Article

pubs.acs.org/journal/ascecg

Biosynthesized Bimetallic Au–Pd Nanoparticles Supported on TiO_2 for Solvent-Free Oxidation of Benzyl Alcohol

Yingling Hong,[†] Xiaolian Jing,[‡] Jiale Huang,*[,†] Daohua Sun,[†] Tareque Odoom-Wubah,[†] Feng Yang,[†] Mingming Du,[†] and Qingbiao Li*[,†,‡,§,∥]

[†]Department of Chemical and Biochemical Engineering, College of Chemistry and Chemical Engineering, [‡]Environmental Science Research Center, College of the Environment & Ecology, and [§]National Engineering Laboratory for Green Chemical Productions of Alcohols, Ethers and Esters, Xiamen University, Xiamen, 361005, P. R. China

[∥]College of Chemistry & Life Science, Quanzhou Normal University, Quanzhou, 362000, P. R. China

Supporting Information

ABSTRACT: A green bioreductive approach with *Cacumen Platycladi* (*CP*) extract was adopted to fabricate bimetallic Au–Pd/TiO_2 catalysts for solvent-free oxidation of benzyl alcohol (BzOH) to benzaldehyde (BzH) with molar oxygen at atmospheric pressure. The Au–Pd nanoparticles (NPs) before being immobilized onto TiO_2 were determined by transmission electron microscopy. And, the catalysts were further analyzed by X-ray diffraction, X-ray photoelectron spectroscopy, thermogravimetric analysis, etc. Effects of Au/Pd molar ratio, preparation conditions, and reaction conditions on the catalytic activity of Au–Pd/TiO_2 were investigated. And, the Au–Pd/TiO_2 catalyst without calcination that was prepared at 90 °C from the Au–Pd NPs with Au/Pd molar ratio of 2:1 exhibited excellent catalytic performance. With the catalyst, BzOH conversion of 74.2% and selectivity to BzH 95.8% were attained at the reaction temperature of 90 °C with an oxygen flow rate of 90 mL/min. Meanwhile, the recycling tests showed that, after seven recycles, the catalyst still remained with high conversion and selectivity. Therefore, the catalyst had excellent durability and reusability and good prospects for industrial application.

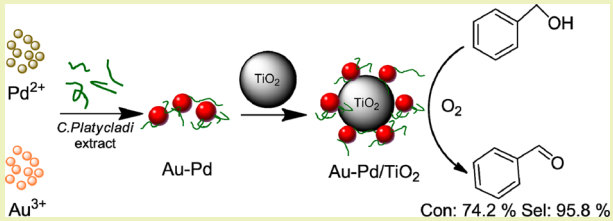

KEYWORDS: *Gold, Palladium, Bioreduction, Benzyl alcohol, Oxidation*

INTRODUCTION

As important precursor or intermediate in chemical industries,[1] benzaldehyde (BzH) is produced mainly through two processes, i.e. the hydrolysis of benzal chloride and toluene oxidation.[2,3] However, the hydrolysis of benzal chloride poses the problem of chlorine contamination while the toluene oxidation led to poor selectivity to BzH. In contrast, direct oxidation of benzyl alcohol (BzOH) in liquid phase can not only circumvent the chlorine contamination but also achieve satisfactory selectivity to BzH. Hence, liquid phase oxidation of BzOH has attracted increasing attention from scientific researchers and industrial community.[4,5] It is more environmentally friendly to produce BzH from the liquid phase but solvent-free oxidation of BzOH in which BzOH plays dual roles as raw material and solvent.

To date, design of efficient catalysts for oxidation of BzOH by proper oxidants has been extensively studied. Expensive and environmentally unfriendly oxidants such as chromium trioxide,[6] ammonium permanganate,[7] and *tert*-butyl hydroperoxide[8] are usually used. Aqueous H_2O_2 have also been used in a few studies because of economic and environmental concerns,[9,10] but it is easy to decompose. Molecular oxygen is desirable because it is a clean and cheap oxidant and, above all, produces water as the sole byproduct.[10]

Noble metal catalysts (Ag, Pt, Pd, Au, Ru, etc.) have been widely used for heterogeneous catalysis in oxidization of alcohols to aldehydes.[11−13] It is urgent to develop a more active catalyst for the solvent-free BzOH oxidation to attain high conversion of BzOH and selectivity to BzH. It is very interesting that bimetallic nanoparticles (NPs) might outperform monometallic ones in catalytic properties due to synergetic effects between two metal components. Synergetic effects in bimetallic nanocatalysts are often introduced by the change of electronic structure due to charge transfer or structural strain between metals, interfacial collaboration by two metals, and interfacial stabilization.[14] For example, Au–Pd catalysts showed better performance for the oxidation of BzOH to BzH, i.e. higher BzOH conversion and BzH selectivity, compared with monometallic catalysts.[15,16] Furthermore, different preparation procedures may lead to variation in the particle size, morphology, structure, and electronic properties of bimetallic nanoparticle catalysts, which significantly affect the metal–support interaction and consequently the catalytic performance. Driven by green chemistry, some researches have been focused on the biosynthesis of NPs using plant

Received: November 18, 2013
Revised: June 5, 2014
Published: June 9, 2014

extract as a natural factory without additional chemicals.[17−23] In some previous studies, $NaBH_4$ and poly(vinyl alcohol) were used as reductant and protecting agent, respectively.[24−26] Furthermore, biosynthesized NPs could be immobilized onto proper supports, giving rise to efficient catalysts for oxidation of carbon monoxide,[27] propylene,[28−30] styrene,[31] and BzOH.[32−34] In our previous study, with *Cacumen Platycladi* (*CP*) extract, Au−Pd bimetallic NPs were synthesized through single-step reduction of Au (III) and Pd (II) precursor with *CP* extract in an aqueous environment.[20] The efficient bimetallic catalysts Au−Pd/MgO for oxidation of BzOH in aqueous medium were prepared based on the biosynthesis.[9]

In this work, alloy Au−Pd/TiO_2 catalysts were prepared through sol-immobilization technique using *CP* extract as bioreducing agent. We focused on the biosynthesis of alloy NPs using *CP* extract as a natural factory without additional chemicals, except for the metal precursors. Then, the catalytic performance of the alloy catalysts for the solvent-free aerobic oxidation of BzOH to BzH (oxygen is chosen as the oxidant) was tested. The influences of various catalyst parameters and catalytic reaction conditions on the alloy catalytic performance of the Au−Pd catalysts were investigated. The bimetallic catalysts are characterized using transmission electron microscopy (TEM), X-ray diffraction (XRD), X-ray photoelectron spectroscopy (XPS), Fourier transform infrared (FT-IR) spectroscopy of adsorbed pyridine, and thermogravimetric (TG) analysis.

EXPERIMENTAL SECTION

Materials. Chloroauric acid ($HAuCl_4$), palladium nitrate ($Pd(NO_3)_2$), and rutile TiO_2 were supplied by Sinopharm Chemical Reagent Co. Ltd. (China). Benzyl alcohol was supplied by Xilong Chemical Reagent Co. Ltd. (China). The same sundried *CP* in the previous study[9] was used in this work.

Preparation of *CP* Extract. The *CP* leaf fine powder was screened with a 20-mesh sieve. Then, 4.0 g screened powder was dispersed in 400 mL deionized (DI) water in a conical flask. The mixture was then shaken at 150 rpm for 4 h at 30 °C and filtrated to get filtrate (10 g L^{-1}) for preparation of the Au−Pd catalysts.

Preparation of Au−Pd/TiO_2 Catalysts. Bimetallic catalysts were prepared via sol-immobilization (SI) method. *CP* extract (20 mL) was added to the aqueous solution (40 mL) of $HAuCl_4$ (0.5 mM) and $Pd(NO_3)_2$ (0.7 mM) under vigorous stirring at 90 °C. After 1 h, 0.6 g TiO_2 was added and kept stirring for another 1 h. Then, the suspension was filtered and washed thoroughly with deionized water and put in a vacuum oven at 50 °C for 12 h.

Catalysts with different Au/Pd molar ratios were prepared by changing the concentrations of $HAuCl_4$ and $Pd(NO_3)_2$. And, they were labeled by the Au/Pd molar ratio. For instance, Au(1)Pd(1)/TiO_2 denoted the catalyst prepared with Au/Pd molar ratio of 1:1. The total metal loading was 2% for all catalysts with different Au/Pd molar ratios.

Characterization of Au-PdNPs and Au−Pd/TiO_2 Catalysts. The details on characterizations with transmission electron microscopy (TEM), X-ray diffraction (XRD), X-ray photoelectron spectroscopy (XPS), Fourier transform infrared (FT-IR) spectroscopy, and thermogravimetric (TG) and differential thermogravimetric (DTG) analysis were the same in our previous work.[9,31,34] C 1s was used as a reference to calibrate the obtained XPS data. The FT-IR spectra of pyridine adsorption studies were obtained at room temperature, wherein the samples (0.06 g) were pressed into thin wafers. And TG and DTG analyses were carried out at a heating rate of 10 K min^{-1} from 303−1273 K.

Catalytic Activity Measurements. Liquid phase oxidation of BzOH with molecular oxygen as the oxidant was carried out in a magnetically stirred three necked flask (50 mL) with reflux condenser and oil bath. And, the oil bath was heated to appropriate temperature in advance. A 0.4 g portion of catalyst was stirred with 20 mL BzOH with continuous oxygen bubbling (controlled by a glass rotameter) at atmospheric pressure. The same procedures on analysis of reaction products with gas chromatography were adopted.[9]

RESULTS AND DISCUSSION

Characterizations of Au−Pd NPs and Au−Pd/TiO_2 Catalysts. TEM was used to characterize the morphology of the Au−Pd NPs and the Au−Pd/TiO_2 catalysts. The images of the Au−Pd NPs with different Au/Pd molar ratio are shown in Figure 1. As illustrated, all of the Au−Pd NPs were spherical and well dispersed, given the same initial metal concentration and the other bioreduction conditions. The histograms of their size distribution and statistic sizes were given in the inset images. Compared with the particle sizes of monometallic Au and Pd NPs (18.3 ± 2.3 and 8.2 ± 1.1 nm, respectively) presented in Figure S1, the particle sizes of the bimetallic Au−Pd NPs were in between, suggesting the formation of the bimetallic NPs. The particle sizes of the Au−Pd NPs decreased with the decrease of Au/Pd molar ratio. In other words, the higher the Pd precursor concentration, the smaller the bimetallic particles formed. This phenomenon was in agreement with the previous work by Hutchings et al. They also

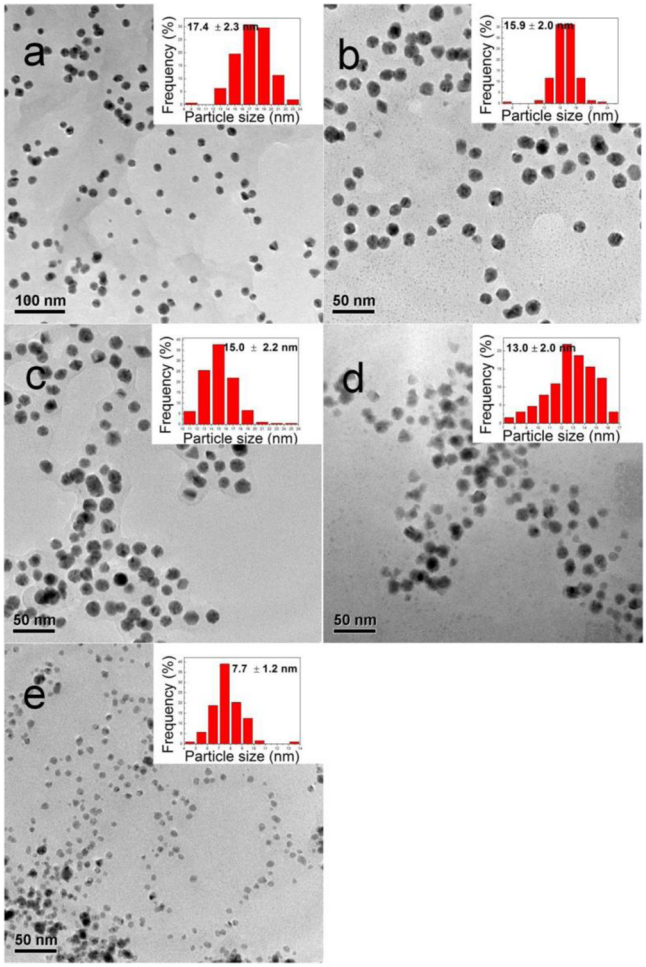

Figure 1. TEM images of bimetallic NPs (preparation conditions: temperature, 90 °C; time, 1 h; and stirring rate, 12 000 rpm) with inset histograms of particle size distributions: (a) Au(7)Pd(1), (b) Au(2)Pd(1), (c) Au(1)Pd(1), (d) Au(1)Pd(2), (e) Au(1)Pd(7) NPs.

dx.doi.org/10.1021/sc500181z | ACS Sustainable Chem. Eng. 2014, 2, 1752−1759

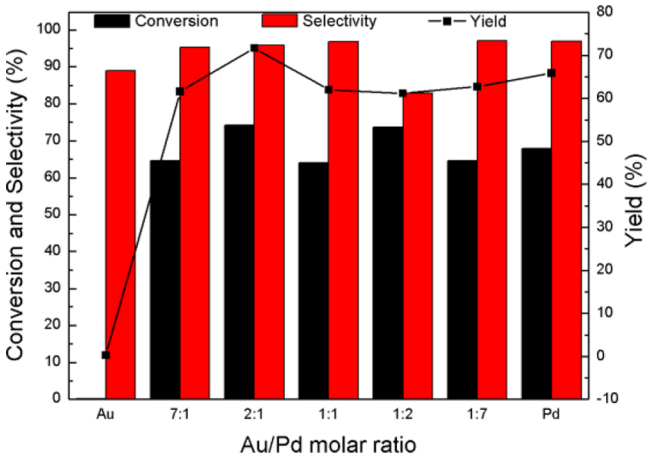

Figure 2. Catalytic performance of Au/TiO_2, Pd/TiO_2, and Au–Pd/TiO_2 catalysts with different Au/Pd molar ratio. Reaction conditions: temperature, 90 °C; O_2 flow rate, 90 mL/min (1 atm); reaction time, 6 h; and stirring rate, 12 000 rpm.

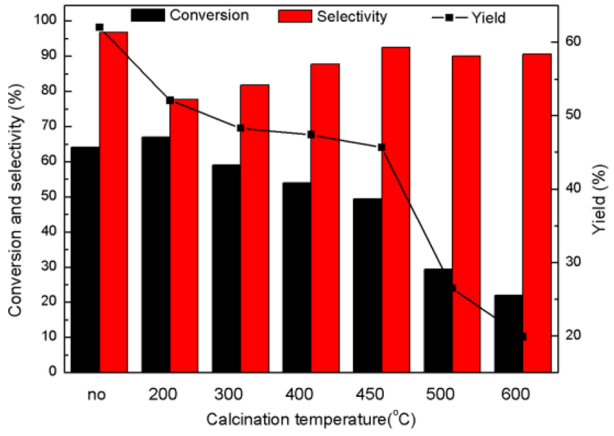

Figure 3. Catalytic performance of Au(1)Pd(1)/TiO_2 catalysts at different calcination temperature. Reaction conditions: temperature, 90 °C; O_2 flow rate, 90 mL/min (1 atm); reaction time, 6 h; and stirring rate, 12 000 rpm.

reported that the smaller NPs comprise largely Pd, and the larger NPs comprise mainly Au in the synthesis of bimetallic Au–Pd NPs.[35] The nature of the bimetallic NPs can be verified through scanning transmission electron microscopy (STEM) and energy-dispersive X-ray (EDX) spectroscopy. The EDX elemental line scanning and STEM images (the inset) of the as-synthesized NPs are presented in the inset images in Figure S2. The results indicated that all the NPs are alloy regardless of different Au/Pd molar ratio. The bimetallic NPs were also observed by high resolution TEM (HRTEM). As shown in Figure S3, the crystal lattice spacing of bimetallic NPs (0.229 nm) was between 0.236 nm (The crystal lattice spacing of Au(111)) and 0.225 nm (The crystal lattice spacing of Pd(111)). Therefore, it provided the evidence that the nanoparticle is an alloy particle of Au and Pd.

XPS technique was employed to analyze the electronic state of metals. The spectra of Au 4f region and Pd 3d region are presented in Figure S4. Figure S4 shows the Au $4f_{7/2}$ signal with a lower position at 83.4 eV, indicating that Au in Au–Pd NPs is metallic phase. Particularly, elemental gold was the sole gold species, revealing complete reduction of Au precursor with *CP* extract. Meanwhile, Figure S4 also shows the Pd $3d_{5/2}$ signal

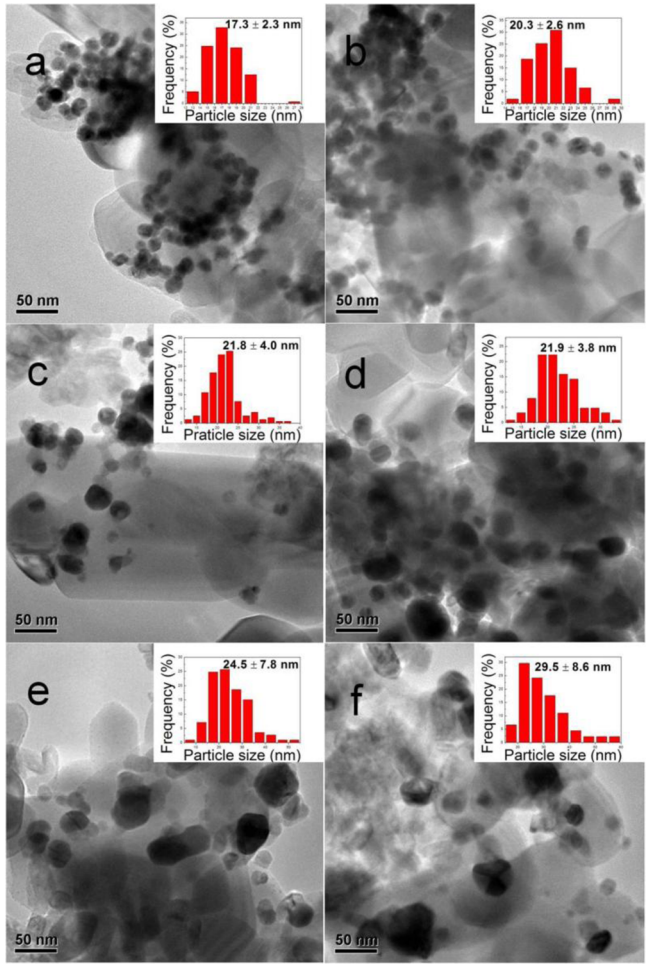

Figure 4. TEM images of Au(1)Pd(1)/TiO_2 catalysts at different calcination temperatures with corresponding sizes distributions. Inset: (a) 200, (b) 300, (c) 400, (d) 450, (e) 500, and (f) 600 °C.

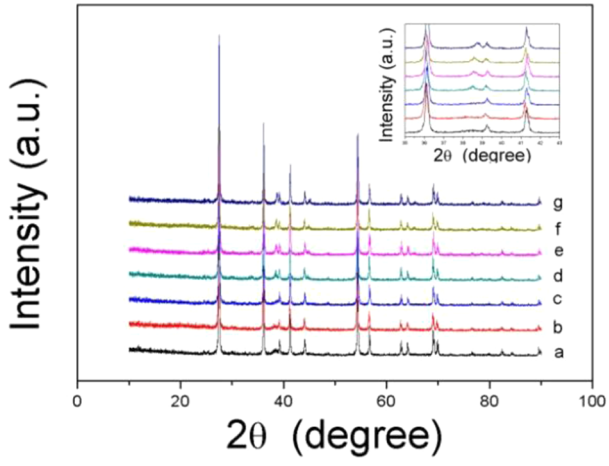

Figure 5. Powder XRD patterns of Au(1)Pd(1)/TiO_2 catalysts at different calcination. Inset: (a) no calcination, (b) 200, (c) 300, (d) 400, (e) 450, (f) 500, and (g) 600 °C.

with a lower position at 334.8 eV, revealing that Pd ions were completely reduced to elemental Pd by the *CP* extract.

TG and DTG analysis were carried out to study the effect of the residual plant biomass on the bioreduction catalysts. The TG profiles are presented in Figure S5. Evidently, the biomass

dx.doi.org/10.1021/sc500181z | *ACS Sustainable Chem. Eng.* 2014, 2, 1752–1759

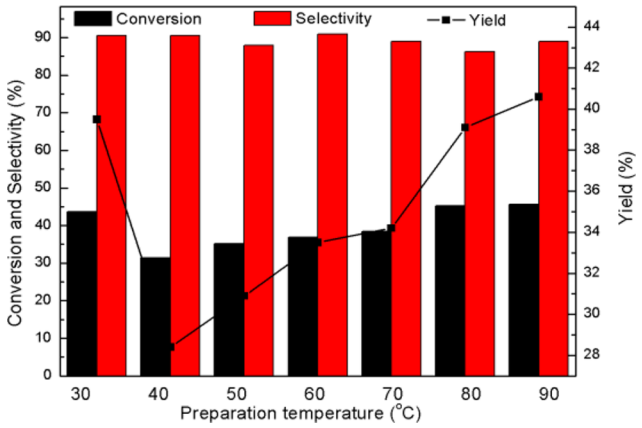

Figure 6. Catalytic performance of Au(2)Pd(1)/TiO_2 with different catalysts preparation temperature. Reaction conditions: temperature, 90 °C; O_2 flow rate, 90 mL/min (1 atm); reaction time, 4 h; and stirring rate, 12 000 rpm.

accounts for 2% weight of the fresh catalysts. We have indicated that reducing sugars, flavones, and polyphenols consisting of most of dry weight of the *CP*,[36] the flavones and reducing sugar also acted as protective agents to prevent the NPs from aggregating[21,37] during the catalyst preparation. The inset DTG profile of the biomass shows that the decomposition temperature was 400−800 K. Therefore, some residual biomolecules played an important role in protecting the bimetallic NPs over the catalysts.

The crystalline phase of the bioreduction catalyst was characterized by powder XRD. Figure S6 exhibits the XRD patterns of Au/TiO_2, Pd/TiO_2, and Au−Pd/TiO_2 catalysts. As shown, the Bragg reflections at 38.1° and 44.3° corresponded to the (111) and (220) of gold. Diffraction peaks at 39.8° and 67.4° attributed are attributed to the (111) and (322) planes of crystalline palladium from the Pd/TiO_2 catalyst are detected. For the bimetallic catalysts, the diffraction peak at 38.6° between Au (111) and Pd (111) can be assigned to the Au−Pd alloy phase.[38,39]

Effect of Au/Pd Molar Ratio. Both monometallic and bimetallic catalysts were tested for the oxidation of BzOH to BzH. Correlations of catalytic activity with the Au/Pd molar ratio are shown in Figure 2. The Au/TiO_2 with Au as active component exhibited extremely low BzOH conversions. However, the Pd catalysts (containing Pd and Au−Pd catalysts) showed much better catalytic activity. The BzOH conversions were within the range of 60−75% while the selectivity to BzH in most cases were higher than 90%. It should be noted that the Au−Pd/TiO_2 in the case of Au/Pd molar ratio of 2:1 exhibited higher BzOH conversion than monometallic Pd/TiO_2 while the selectivity to BzH in the two cases were close. The synergistic interaction between Au and Pd might be responsible for the enhanced BzOH conversion. The addition of small amounts of gold to palladium markedly enhanced the activity of supported Au−Pd NPs because of electronic effect.[35] In contrast with Au/TiO_2, the increase in BzH yields using Au−Pd/TiO_2 could be resulted at all the Au/Pd molar ratios. The highest BzH yield (71.7%) could be achieved at the Au/Pd molar ratio of 2:1, which was 239 times that of the Au/TiO_2 and 1.1 times that of the Pd/TiO_2. As illustrated in Figure 1, two metal in the alloy Au−Pd NPs were well combined and their size fell between those of Au and Pd NPs, given the same initial metal concentration and bioreduction conditions. However, a non-

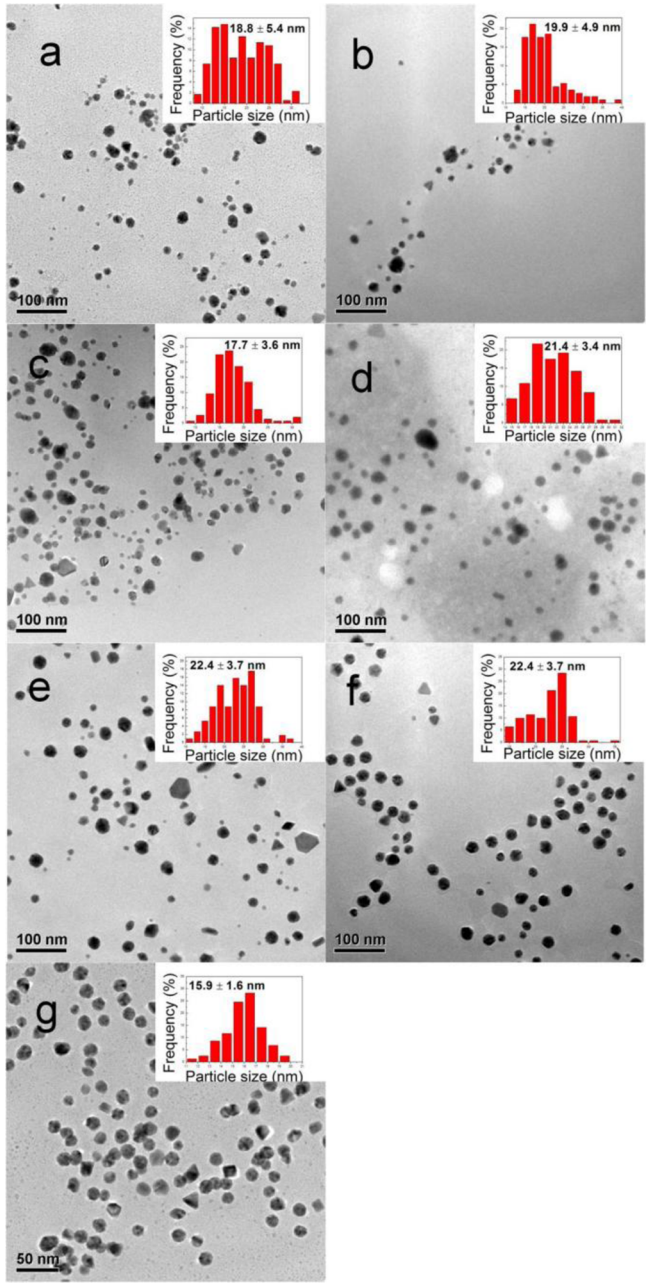

Figure 7. TEM images of Au(2)Pd(1) sols at different preparation temperatures with corresponding sizes distributions. Inset: (a) 30, (b) 40, (c) 50, (d) 60, (e) 70, (f) 80, and (g) 90 °C.

linear relationship can be found between the activity of Au−Pd/TiO_2 and the Au/Pd molar ratio. Compared with the particle sizes of monometallic Au and Pd NPs (18.3 ± 2.3 and 8.2 ± 1.1 nm, respectively) presented in Figure S1, the in between particle size of the alloy Au−Pd NPs shows the chemical combination of Au and Pd atoms to form the alloy NPs. The particle sizes of the Au−Pd NPs decreased with the decrease of Au/Pd molar ratio. In other words, the higher the Pd precursor concentration, the smaller the alloy particles formed. The benzyl alcohol conversion first increases and then decreases with the decreasing alloy size (or the decreasing the Au/Pd molar ratio). It can be seen that the BzOH conversion was associated with the Au/Pd molar ratio and the alloy size. However, the effect of change of the number of atom at the catalyst surface with changing the alloy size remained unclear.

dx.doi.org/10.1021/sc500181z | *ACS Sustainable Chem. Eng.* 2014, 2, 1752−1759

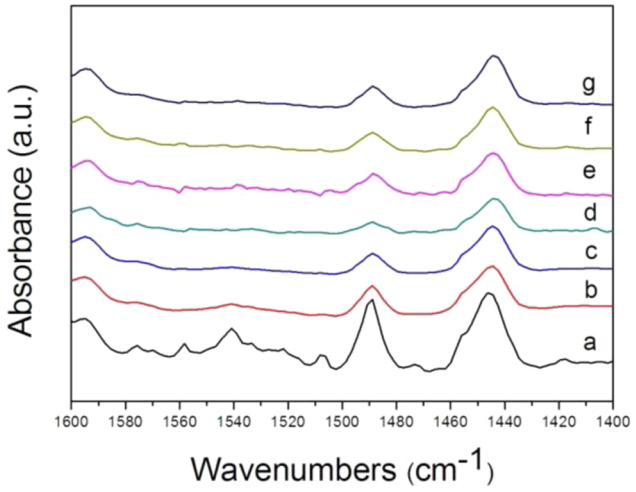

Figure 8. FT-IR spectroscopy of adsorption pyridine on the bimetallic Au−Pd NPs at the Au/Pd molar ratio of 2:1 at different preparation temperatures: (a) 30, (b) 40, (c) 50, (d) 60, (e) 70, (f) 80, and (g) 90 °C.

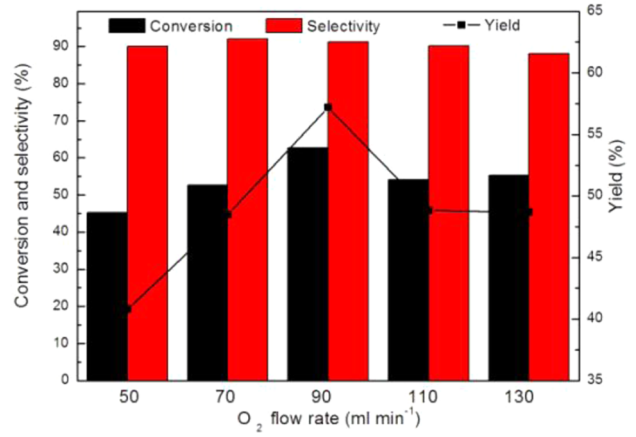

Figure 9. Catalytic performance of Au(2)Pd(1)/TiO_2 with different oxygen flow rate. Reaction conditions: temperature, 90 °C; reaction time, 5 h; and stirring rate, 12 000 rpm.

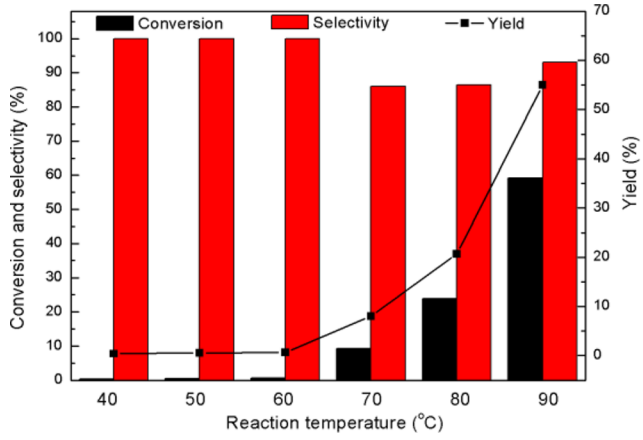

Figure 10. Catalytic performance of Au(2)Pd(1)/TiO_2 with different reaction temperature. Reaction conditions: O_2 flow rate, 90 mL/min (1 atm); reaction time, 5 h; and stirring rate, 12 000 rpm.

Effect of Calcination Temperature. The catalytic activities of the Au−Pd/TiO_2 catalysts calcined at different temperatures are shown in Figure 3. The catalysts showed high selectivity toward BzH (almost 90%), with trace benzoic acid and toluene and benzoate as byproducts, regardless of calcination temperature. However, the calcination was detrimental to the catalytic activity, especially the conversion of BzOH. For instance, the conversion of BzOH was as low as 22% if the Au−Pd/TiO_2 was subjected to calcination at 600 °C. On the contrary, the catalysts without calcination exhibited the highest BzOH conversion, suggesting that calcination at higher temperature was adverse to the formation of high active Au−Pd species. The phenomenon may be explained by the results based on TEM, XRD, and TG characterizations. The TEM images of the catalysts after calcinations at different temperatures are shown in Figure 4. It can be seen that the particle sizes increased with increasing the calcination temperature. As a result, the activity of the bimetallic catalysts decreased with increasing calcination temperature as the surface area decreased after the calcinations. In other words, the calcined nanoparticles tended to sinter. The uncalcined Au−Pd particle sizes were 15.1 ± 2.1 nm (Figure S8), the Au−Pd particle size increased up to 29.5 ± 8.6 nm with less homogeneous dispersion and shape at 600 °C (Figure 4f), which was probably responsible for the very low activity. The XRD patterns for the bimetallic catalysts calcined at different temperatures are shown in Figure 5. As discussed above, the diffraction peaks of the bimetallic catalysts at 38.6°, which located between Au (111) and Pd (111), can be attributed to the Au−Pd alloy phase. The diffraction peaks of Au−Pd/TiO_2 after the calcinations treatment below 400 °C were weak, while the peaks at higher calcined temperature became stronger. Therefore, the particles with larger sizes were formed with the increase of the calcination temperature. The TG analyses of the catalysts calcined at different temperature are shown in Figure S5. Further, the TG results revealed a gradual decrease of plant biomass amount with increasing the calcination temperature (50−600 °C). The activity of the bimetallic catalysts decreased after decomposing some residual biomass as the residual biomass might prevent the bimetallic NPs from agglomeration. Therefore, the increase in the particle size and the loss of plant biomass gave rise to the poor performance of the catalysts calcined at higher temperatures.[9,26]

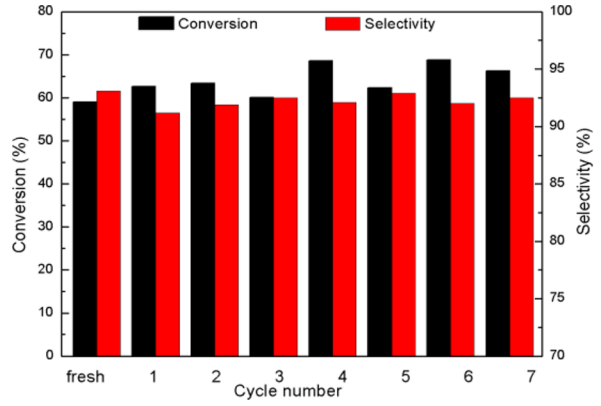

Figure 11. Catalytic performance of recycling bioreduction Au(2)-Pd(1)/TiO_2 catalysts. Reaction conditions: temperature, 90 °C; O_2 flow rate, 90 mL/min (1 atm); reaction time, 5 h; and stirring rate, 12 000 rpm.

Effect of the Catalysts Preparation Temperature. The effect of preparation temperature of the Au−Pd/TiO_2 catalysts on the solvent-free oxidation of BzOH was examined using

Table 1. Comparison of BzOH Oxidation Catalyzed by Bimetallic and Monometallic Catalysts

catalyst	selectivity to BzH (%)	yield[a] (%)	TOF[b] (h^{-1})	reaction temperatue (°C)	reaction time (h)	ref
Au−Pd/TiO_2	95.8	71.7	589	90	6	This work
Au/TiO_2	73.7	39	6348	160	6	25
Au/SBA	86.1	2	1937	140	1	16
Au/HMS	95	41	98	80	2	43
Pd/NMC	91.2	59.8	14 939	160	1	44
Pd/CeO_2	88.9	20.8	17 572	160	1	45
Pd/SBA	90.2	8.6	3701	140	1	16
Au−Pd/TiO_2	70	19.3	20 480	140	0.5	46
Au−Pd/TiO_2	82.8	1	65 400	100	0.5	47
Au−Pd/TiO_2	91	34.2	6767	140	1.4	48
Au−Pd/SBA	90	67.2	6500	160	4	49

[a]Yield = the product of BzOH conversion and BzH selectivity. [b]Measured on the basis of ratio of moles of converted BzOH per mole of metal per hour.

Au−Pd/TiO_2 at the Au/Pd molar ratio of 2:1. It can be seen from Figure 6 that the BzOH conversion increased but the selectivity to BzH remained almost the same with increasing the preparation temperature (except the temperature of 30 °C). Particularly, the BzOH conversion was only 31% at 40 °C due to thermal effect.[34] Therefore, high preparation temperature favored the reaction as the BzOH conversion increased from 31% to 45.6% when the temperature was switched from 40 to 90 °C. However, the better activity was obtained when the temperature was 30 °C. The TEM images of the Au−Pd bimetallic NPs prepared at different temperature are shown in Figure 7. As shown, the particle sizes were around 20 nm. The EDX elemental line scannings of the as-synthesized NPs are shown in Figure S7, and their STEM images are also presented in the inset images in Figure S7. All the as-prepared particles were bimetallic NPs at all the temperatures. FT-IR spectra of adsorbed pyridine are showed in Figure 8. The spectrum contained several significant peaks at 1450, 1490, and 1540 cm^{-1}, which could be assigned to the chemisorption of molecular pyridine at different type of surface acidic sites. The peaks at 1450 cm^{-1} were resulted from the interaction of pyridine with Lewis acidic sites. Meanwhile, the peaks at 1490 cm^{-1} were due to the vibration of pyridine adsorbed on Bronsted acidic and on Lewis acidic sites. The peaks at 1540 cm^{-1} can be attributed to the protonation of pyridine molecule by the Bronsted acidic sites (surface-bound hydroxyl groups).[40,41] And, the peaks at 1540 cm^{-1} only existed in the catalysts prepared at 30 °C. These strong Bronsted and Lewis acidic sites may provide better adsorption centers for reactant molecules,[42] and the low preparation temperature induced plenty of strong Bronsted acidic sites on the TiO_2 surface. The catalysts prepared at 30 °C exhibited good catalytic performance, which was due to the strong Bronsted acidic sites on the surface of TiO_2.

Effect of Oxygen Flow Rate. Effect of oxygen flow rate (50−130 mL/min) on the catalytic reaction was investigated, and the results are showed in Figure 9. Increasing the oxygen flow rate from 50 to 90 mL/min had linear effect BzOH conversion and BzH yield. In addition, BzH selectivity was not affected at high O_2 flow rate and remained constant, while a little toluene and benzoic acid and benzyl benzoate were formed. However, the BzOH conversion decreased and BzH selectivity remained at about 90% with 110 and 130 mL/min flow rate. The conversion decline at 110 mL/min could be attributed to low utilization of oxygen by flowing too fast to react with BzOH substances. The best activity was achieved at a flow rate of 90 mL/min.

Effect of Reaction Temperature. The effect of reaction temperature on the aerobic oxidation of BzOH is shown in Figure 10 using the Au(2)Pd(1)/TiO_2 catalysts (40, 50, 60, 70, 80, and 90 °C). The BzH selectivity was high (above 86%), whereas the BzOH conversion depended on the reaction temperature. A poor conversion (below 1%) was obtained at low reaction temperature (40, 50, and 60 °C) as the oxidation of BzOH is an endothermic reaction. As expected, the elevated temperature led to the remarkable enhancement in both BzOH conversion and BzH yield. The BzOH conversion and BzH selectivity were 59.2% and 93.1%, respectively, at the temperature of 90 °C. As the reaction temperature increased from 70 to 90 °C, the BzOH conversion and BzH selectivity increased, implying that a higher reaction temperature promoted the oxidation of BzOH and inhibited the disproportionation of BzOH. Obviously, the moderate reaction temperature of 90 °C provided the highest BzH yield (55.08%).

Durability of the Bioreduction Catalysts. Durability of heterogeneous catalysts is an important aspect that should be considered for industrial application. Recycle tests were carried out to assess the durability of the Au(2)Pd(1)/TiO_2 catalysts. The catalysts after reaction were recovered by centrifugation, washed thoroughly with ethanol and deionized water, and then dried and reused for another reaction under the same conditions. As shown in Figure 11, the conversion of BzOH and selectivity of BzH remained almost the same during seven cycles, indicating the very high stability of the alloy catalysts. Figure S9 shows the XRD patterns of the fresh catalyst and seven cycles catalyst, we can observe that the intensity of the diffraction peaks kept almost the same after seven cycles. The plant biomass might adhere to the alloy NPs to prevent the metal leaching. Therefore, the residual biomass indeed contributed to remarkable durability of the bioreduction alloy catalysts.

Comparison of Bioreduction Catalysts with Analogous Catalysts. The yield of BzH and the TOF for solvent-free oxidation with the bioreduction Au−Pd alloy catalysts herein and other Au, Pd or Au−Pd based catalysts reported in the literature are compared in Table 1. Obviously, the catalytic performance of the Au−Pd alloy catalysts herein was comparable and superior to those by conventional chemical methods (DP, impregnation, etc.). Both high BzH yield and fair TOF values were attained with the bioreduction Au−Pd alloy catalysts. Higher TOF values were obtained at very high

reaction temperatures in the literatures, as BzOH oxidation is an endothermic reaction. However, high reaction temperature means more energy consumption. Considering the trade-off between catalytic performance and energy consumption, our catalysts are more efficient compared with those in the literatures.

CONCLUSIONS

In conclusion, a green process bimetallic Au−Pd/TiO_2 catalyst assisted by bioreduction for solvent-free oxidation of BzOH to BzH with was investigated in this work. The most appropriate conditions, catalysts preparation temperature of 90 °C, Au/Pd molar ratio of 2:1, catalyst without calcination, reaction time of 6 h, temperature of 90 °C, oxygen flow rate of 90 mL/min, were obtained. The bimetallic catalysts were reusable for up to seven runs consecutively and remained high activity and selectivity. The plant biomass endowed the catalyst with the remarkable durability of the bioreduction catalyst. Therefore, the as-prepared bimetallic catalyst is promising for industrial application.

ASSOCIATED CONTENT

Supporting Information

Details of experiment results, such as TEM images, high resolution TEM images, EDX elemental line scanning, TG and DTG profiles, XPS spectra, and XRD patterns. This material is available free of charge via the Internet at http://pubs.acs.org/

AUTHOR INFORMATION

Corresponding Authors

*E-mail: cola@xmu.edu.cn (J.H.)
*E-mail: kelqb@xmu.edu.cn (Q.L.).

Notes

The authors declare no competing financial interest.

ACKNOWLEDGMENTS

This work was supported by the national Nature Science Foundation of China (NSFC Project No.21036004) and the fund of the State Key Laboratory of Advanced Technologies for Comprehensive Utilization of Platinum Metals (SKL-SPM-201210).

REFERENCES

(1) Yu, Y.; Lu, B.; Wang, X.; Zhao, J.; Wang, X.; Cai, Q. Highly selective oxidation of benzyl alcohol to benzaldehyde with hydrogen peroxide by biphasic catalysis. *Chem. Eng. J.* **2010**, *162*, 738−742.
(2) Choudhary, V. R.; Chaudhari, P. A.; Narkhede, V. S. Solvent-free liquid phase oxidation of benzyl alcohol to benzaldehyde by molecular oxygen using non-noble transition metal containing hydrotalcite-like solid catalysts. *Catal. Commun.* **2003**, *4*, 171−175.
(3) Martin, A.; Bentrup, U.; Brückner, A.; Lücke, B. Catalytic performance of vanadyl pyrophosphate in the partial oxidation of toluene to benzaldehyde. *Catal. Lett.* **1999**, *59*, 61−65.
(4) Bavykin, D. V.; Lapkin, A. A.; Kolaczkowski, S. T.; Plucinski, P. K. Selective oxidation of alcohols in a continuous multifunctional reactor: Ruthenium oxide catalysed oxidation of benzyl alcohol. *Appl. Catal., A* **2005**, *288*, 175−184.
(5) Choudhary, V. R.; Jha, R.; Jana, P. Solvent-free selective oxidation of benzyl alcohol by molecular oxygen over uranium oxide supported nano-gold catalyst for the production of chlorine-free benzaldehyde. *Green Chem.* **2007**, *9*, 267.
(6) González-Núñez, M. E.; Mello, R.; Olmos, A.; Acerete, R.; Asensio, G. Oxidation of Alcohols to Carbonyl Compounds with CrO_3·SiO_2 in Supercritical Carbon Dioxide. *J. Org. Chem.* **2006**, *71*, 1039−1042.
(7) Kotai, L.; Kazinczy, B.; Keszler, A.; Holly, S.; Gacs, I.; Banerji, K. Three reagents in one: Ammonium permanganate in the oxidation of benzyl alcohol. *J. Chem. Sci.* **2001**, *56*, 823−825.
(8) Behera, G. C.; Parida, K. M. Liquid phase catalytic oxidation of benzyl alcohol to benzaldehyde over vanadium phosphate catalyst. *Appl. Catal., A* **2012**, *413−414*, 245−253.
(9) Zhan, G.; Hong, Y.; Mbah, V. T.; Huang, J.; Ibrahim, A.-R.; Du, M.; Li, Q. Bimetallic Au−Pd/MgO as efficient catalysts for aerobic oxidation of benzyl alcohol: A green bio-reducing preparation method. *Appl. Catal., A* **2012**, *439−440*, 179−186.
(10) Choudhary, V. R.; Dhar, A.; Jana, P.; Jha, R.; Uphade, B. S. A green process for chlorine-free benzaldehyde from the solvent-free oxidation of benzyl alcohol with molecular oxygen over a supported nano-size gold catalyst. *Green Chem.* **2005**, *7*, 768.
(11) Mallat, T.; Baiker, A. Oxidation of alcohols with molecular oxygen on solid catalysts. *Chem. Rev.* **2004**, *104*, 3037−3058.
(12) Ferri, D.; Mondelli, C.; Krumeich, F.; Baiker, A. Discrimination of active palladium sites in catalytic liquid-phase oxidation of benzyl alcohol. *J. Phys. Chem. B* **2006**, *110*, 22982−22986.
(13) Hosokawa, S.; Hayashi, Y.; Imamura, S.; Wada, K.; Inoue, M. Effect of the Preparation Conditions of Ru/CeO2 Catalysts for the Liquid Phase Oxidation of Benzyl Alcohol. *Catal. Lett.* **2009**, *129*, 394−399.
(14) Wu, B. H.; Zheng, N. F. Surface and interface control of noble metal nanocrystals for catalytic and electrocatalytic applications. *Nano Today* **2013**, *8*, 168−197.
(15) Marx, S.; Baiker, A. Beneficial interaction of gold and palladium in bimetallic catalysts for the selective oxidation of benzyl alcohol. *J. Phys. Chem. C* **2009**, *113*, 6191−6201.
(16) Chen, Y.; Lim, H.; Tang, Q.; Gao, Y.; Sun, T.; Yan, Q.; Yang, Y. Solvent-free aerobic oxidation of benzyl alcohol over Pd monometallic and Au−Pd bimetallic catalysts supported on SBA-16 mesoporous molecular sieves. *Appl. Catal., A* **2010**, *380*, 55−65.
(17) Shankar, S. S.; Rai, A.; Ankamwar, B.; Singh, A.; Ahmad, A.; Sastry, M. Biological synthesis of triangular gold nanoprisms. *Nat. Mater.* **2004**, *3*, 482−488.
(18) Xie, J.; Lee, J. Y.; Wang, D. I.; Ting, Y. P. Identification of Active Biomolecules in the High-Yield Synthesis of Single-Crystalline Gold Nanoplates in Algal Solutions. *Small* **2007**, *3*, 672−682.
(19) Xie, J. P.; Lee, J. Y.; Wang, D. I. C.; Ting, Y. P. Silver nanoplates: From biological to biomimetic synthesis. *ACS Nano* **2007**, *1*, 429−439.
(20) Zhan, G. W.; Huang, J. L.; Du, M. M.; Abdul-Rauf, I.; Ma, Y.; Li, Q. B. Green synthesis of Au-Pd bimetallic nanoparticles: Single-step bioreduction method with plant extract. *Mater. Lett.* **2011**, *65*, 2989−2991.
(21) Huang, J. L.; Zhan, G. W.; Zheng, B. Y.; Sun, D. H.; Lu, F. F.; Lin, Y.; Chen, H. M.; Zheng, Z. D.; Zheng, Y. M.; Li, Q. B. Biogenic Silver Nanoparticles by Cacumen Platycladi Extract: Synthesis, Formation Mechanism, and Antibacterial Activity. *Ind. Eng. Chem. Res.* **2011**, *50*, 9095−9106.
(22) Zheng, B.; Kong, T.; Jing, X.; Odoom-Wubah, T.; Li, X.; Sun, D.; Lu, F.; Zheng, Y.; Huang, J.; Li, Q. Plant-mediated synthesis of platinum nanoparticles and its bioreductive mechanism. *J. Colloid Interface Sci.* **2013**, *396*, 138−145.
(23) Zhou, Y.; Lin, W. S.; Huang, J. L.; Wang, W. T.; Gao, Y. X.; Lin, L. Q.; Li, Q. B.; Lin, L.; Du, M. M. Biosynthesis of Gold Nanoparticles by Foliar Broths: Roles of Biocompounds and Other Attributes of the Extracts. *Nanoscale. Res. Lett.* **2010**, *5*, 1351−1359.
(24) Pritchard, J.; Kesavan, L.; Piccinini, M.; He, Q.; Tiruvalam, R.; Dimitratos, N.; Lopez-Sanchez, J. A.; Carley, A. F.; Edwards, J. K.; Kiely, C. J.; Hutchings, G. J. Direct synthesis of hydrogen peroxide and benzyl alcohol oxidation using Au-Pd catalysts prepared by sol immobilization. *Langmuir* **2010**, *26*, 16568−77.
(25) Dimitratos, N.; Lopez-Sanchez, J. A.; Morgan, D.; Carley, A.; Prati, L.; Hutchings, G. J. Solvent free liquid phase oxidation of benzyl alcohol using Au supported catalysts prepared using a sol immobilization technique. *Catal. Today* **2007**, *122*, 317−324.

(26) Dimitratos, N.; Lopez-Sanchez, J. A.; Morgan, D.; Carley, A. F.; Tiruvalam, R.; Kiely, C. J.; Bethell, D.; Hutchings, G. J. Solvent-free oxidation of benzyl alcohol using Au-Pd catalysts prepared by sol immobilisation. *Phys. Chem. Chem. Phys.* **2009**, *11*, 5142−53.
(27) Vilchis-Nestor, A.; Avalos-Borja, M.; Gómez, S.; Hernández, J. A.; Olivas, A.; Zepeda, T. Alternative bio-reduction synthesis method for the preparation of Au (AgAu)/SiO_2−Al_2O_3 catalysts: Oxidation and hydrogenation of CO. *Appl. Catal., B* **2009**, *90*, 64−73.
(28) Du, M. M.; Zhan, G. W.; Yang, X.; Wang, H. X.; Lin, W. S.; Zhou, Y.; Zhu, J.; Lin, L.; Huang, J. L.; Sun, D. H.; Jia, L. S.; Li, Q. B. Ionic liquid-enhanced immobilization of biosynthesized Au nanoparticles on TS-1 toward efficient catalysts for propylene epoxidation. *J. Catal.* **2011**, *283*, 192−201.
(29) Zhan, G. W.; Du, M. M.; Huang, J. L.; Li, Q. B. Green synthesis of Au/TS-1 catalysts via two novel modes and their surprising performance for propylene epoxidation. *Catal. Commun.* **2011**, *12*, 830−833.
(30) Zhan, G. W.; Du, M. M.; Sun, D. H.; Huang, J. L.; Yang, X.; Ma, Y.; Ibrahim, A. R.; Li, Q. B. Vapor-Phase Propylene Epoxidation with H_2/O_2 over Bioreduction Au/TS-1 Catalysts: Synthesis, Characterization, and Optimization. *Ind. Eng. Chem. Res.* **2011**, *50*, 9019−9026.
(31) Huang, J.; Liu, C.; Sun, D.; Hong, Y.; Du, M.; Odoom-Wubah, T.; Fang, W.; Li, Q. Biosynthesized gold nanoparticles supported over TS-1 toward efficient catalyst for epoxidation of styrene. *Chem. Eng. J.* **2014**, *235*, 215−223.
(32) Zhan, G. W.; Hong, Y. L.; Lu, F. F.; Ibrahim, A. R.; Du, M. M.; Sun, D. H.; Huang, J. L.; Li, Q. B.; Li, J. Kinetics of liquid phase oxidation of benzyl alcohol with hydrogen peroxide over bio-reduced Au/TS-1 catalysts. *J. Mol. Catal. A-Chem.* **2013**, *366*, 215−221.
(33) Zhan, G. W.; Hong, Y. L.; Mbah, V. T.; Huang, J. L.; Ibrahim, A. R.; Du, M. M.; Li, Q. B. Bimetallic Au-Pd/MgO as efficient catalysts for aerobic oxidation of benzyl alcohol: A green bio-reducing preparation method. *Appl. Catal., A* **2012**, *439*, 179−186.
(34) Zhan, G. W.; Huang, J. L.; Du, M. M.; Sun, D. H.; Abdul-Rauf, I.; Lin, W. S.; Hong, Y. L.; Li, Q. B. Liquid phase oxidation of benzyl alcohol to benzaldehyde with novel uncalcined bioreduction Au catalysts: High activity and durability. *Chem. Eng. J.* **2012**, *187*, 232−238.
(35) Hutchings, G. J.; Kiely, C. J. Strategies for the Synthesis of Supported Gold Palladium Nanoparticles with Controlled Morphology and Composition. *Acc. Chem. Res.* **2013**, *46*, 1759−1772.
(36) Jiang, X.; Sun, D.; Zhang, G.; He, N.; Liu, H.; Huang, J.; Odoom-Wubah, T.; Li, Q. Investigation of active biomolecules involved in the nucleation and growth of gold nanoparticles by Artocarpus heterophyllus Lam leaf extract. *J. Nanopart. Res.* **2013**, *15*, 1741.
(37) Zhan, G. W.; Huang, J. L.; Lin, L. Q.; Lin, W. S.; Emmanuel, K.; Li, Q. B. Synthesis of gold nanoparticles by Cacumen Platycladi leaf extract and its simulated solution: toward the plant-mediated biosynthetic mechanism. *J. Nanopart. Res.* **2011**, *13*, 4957−4968.
(38) Devarajan, S.; Bera, P.; Sampath, S. Bimetallic nanoparticles: a single step synthesis, stabilization, and characterization of Au-Ag, Au-Pd, and Au-Pt in sol-gel derived silicates. *J. Colloid Interface Sci.* **2005**, *290*, 117−29.
(39) Ma, C. Y.; Dou, B. J.; Li, J. J.; Cheng, J.; Hu, Q.; Hao, Z. P.; Qiao, S. Z. Catalytic oxidation of benzyl alcohol on Au or Au−Pd nanoparticles confined in mesoporous silica. *Appl. Catal., B* **2009**, *92*, 202−208.
(40) Busch, O. M.; Brijoux, W.; Thomson, S.; Schüth, F. Spatially resolving infrared spectroscopy for parallelized characterization of acid sites of catalysts via pyridine sorption: Possibilities and limitations. *J. Catal.* **2004**, *222*, 174−179.
(41) Davis, B. H.; Keogh, R. A.; Alerasool, S.; Zalewski, D. J.; Day, D. E.; Doolin, P. K. Infrared study of pyridine adsorbed on unpromoted and promoted sulfated zirconia. *J. Catal.* **1999**, *183*, 45−52.
(42) Wang, X.; Yu, J. C.; Liu, P.; Wang, X.; Su, W.; Fu, X. Probing of photocatalytic surface sites on SO42−/TiO2 solid acids by in situ FT-IR spectroscopy and pyridine adsorption. *J. Photochem. Photobiol. A* **2006**, *179*, 339−347.
(43) Ma, C. Y.; Cheng, J.; Wang, H. L.; Hu, Q.; Tian, H.; He, C.; Hao, Z. P. Characteristics of Au/HMS catalysts for selective oxidation of benzyl alcohol to benzaldehyde. *Catal. Today* **2010**, *158*, 246−251.
(44) Wang, B.; Lin, M.; Ang, T. P.; Chang, J.; Yang, Y.; Borgna, A. Liquid phase aerobic oxidation of benzyl alcohol over Pd and Rh catalysts on N-doped mesoporous carbon: Effect of the surface acido-basicity. *Catal. Commun.* **2012**, *25*, 96−101.
(45) Chen, Y.; Zheng, H.; Guo, Z.; Zhou, C.; Wang, C.; Borgna, A.; Yang, Y. Pd catalysts supported on MnCeOx mixed oxides and their catalytic application in solvent-free aerobic oxidation of benzyl alcohol: Support composition and structure sensitivity. *J. Catal.* **2011**, *283*, 34−44.
(46) Miedziak, P. J.; He, Q.; Edwards, J. K.; Taylor, S. H.; Knight, D. W.; Tarbit, B.; Kiely, C. J.; Hutchings, G. J. Oxidation of benzyl alcohol using supported gold−palladium nanoparticles. *Catal. Today* **2011**, *163*, 47−54.
(47) Enache, D. I.; Barker, D.; Edwards, J. K.; Taylor, S. H.; Knight, D. W.; Carley, A. F.; Hutchings, G. J. Solvent-free oxidation of benzyl alcohol using titania-supported gold−palladium catalysts: Effect of Au−Pd ratio on catalytic performance. *Catal. Today* **2007**, *122*, 407−411.
(48) Cao, E.; Sankar, M.; Nowicka, E.; He, Q.; Morad, M.; Miedziak, P. J.; Taylor, S. H.; Knight, D. W.; Bethell, D.; Kiely, C. J.; Gavriilidis, A.; Hutchings, G. J. Selective suppression of disproportionation reaction in solvent-less benzyl alcohol oxidation catalysed by supported Au−Pd nanoparticles. *Catal. Today* **2013**, *203*, 146−152.
(49) Chen, Y.; Wang, H.; Liu, C.-J.; Zeng, Z.; Zhang, H.; Zhou, C.; Jia, X.; Yang, Y. Formation of monometallic Au and Pd and bimetallic Au−Pd nanoparticles confined in mesopores via Ar glow-discharge plasma reduction and their catalytic applications in aerobic oxidation of benzyl alcohol. *J. Catal.* **2012**, *289*, 105−117.